

Article

Fretting Wear Behaviors of Aluminum Cable Steel Reinforced (ACSR) Conductors in High-Voltage Transmission Line

Xingchi Ma ^{1,*}, Lei Gao ¹, Junxi Zhang ¹ and Lai-Chang Zhang ^{2,*}

¹ Shanghai Key Laboratory of Materials Protection and Advanced Materials in Electric Power, Shanghai University of Electric Power, Shanghai 200090, China; gaolei20112762@163.com (L.G.); zhangjunxi@shiep.edu.cn (J.Z.)

² School of Engineering, Edith Cowan University, 270 Joondalup Drive, Joondalup, Perth, WA 6027, Australia

* Correspondence: maxingchi@shiep.edu.cn (X.M.); lc Zhangimr@gmail.com or l.zhang@ecu.edu.au (L.-C.Z.); Tel.: +86-21-3530-3902 (X.M.); +61-8-6304-2322 (L.-C.Z.)

Received: 9 August 2017; Accepted: 12 September 2017; Published: 14 September 2017

Abstract: This work reports the fretting wear behavior of aluminum cable steel reinforced (ACSR) conductors for use in high-voltage transmission line. Fretting wear tests of Al wires were conducted on a servo-controlled fatigue testing machine with self-made assistant apparatus, and their fretting process characteristics, friction force, wear damage, and wear surface morphology were detailed analyzed. The results show that the running regime of Al wires changes from a gross slip regime to a mixed regime more quickly as increasing contact load. With increasing amplitudes, gross slip regimes are more dominant under contact loads of lower than 30 N. The maximum friction force is relatively smaller in the NaCl solution than in a dry friction environment. The primary wear mechanisms in dry friction environments are abrasive wear and adhesive wear whereas abrasive wear and fatigue damage are dominant in NaCl solution.

Keywords: ACSR conductors; fretting wear; fretting corrosion; wear mechanism

1. Introduction

Aluminum cable steel reinforced (ACSR) conductors are extensively used in electric transmission systems in different countries and regions, especially in China. Because of being operated in wild environments, ACSR conductors are usually subject to fretting damage by wind excitation and atmospheric corrosion by industrial pollution and salty environments. As a type of critical component of high-voltage transmission systems, most ACSR conductors have been operated for 30–45 years, approaching to their middle life, thereby requiring very high maintenance costs [1–6]. Therefore, it is significant to explore fretting damage behaviors of ACSR conductors in dry and corrosive conditions.

Fretting is the movement in small amplitude (usually in micrometers) between two contact surfaces and it is affected by very complicated factors [7,8]. In recent years, many endeavors have been made on fretting damage behavior of ACSR conductors. Zhou et al. [9,10] focused on the fretting fatigue behaviors of ACSR conductors and found that fretting caused plastic deformation, wear and cracking, then finally fatigue failure. Studies on the damage of 26-year-old ACSR conductors in the 100 kV Zhu-Xie electric transmission system in China revealed that adhesion/abrasive fretting damage mechanisms and fatigue cracks propagation were dominated in the inner Al wires [11]. Zhang et al. [12–16] studied the fretting fatigue failure behavior of hoisting rope in different environments and found that alkaline media can accelerate rope damage in their fretting running. According to the literatures [17–28], metals exposed to different surroundings display different corrosion rates because of different types of corrosive ions in such surroundings. Considering those

coastal regions where many high-voltage transmission lines are operated, which are subjected to severe damage caused by the interaction between corrosive medium and fretting wear [29–35], it is necessary to investigate the fretting wear behaviors of ACSR conductors in marine environments which may be a problem for ACSR conductors in these areas.

The primary aim of the present study is to investigate the fretting wear behaviors of ACSR Al wire. Fretting wear tests of Al wire were carried out on the test rig. This work explored the fretting wear behaviors of Al wire in an ACSR conductor under different amplitudes and contact loads. The morphologies of contact scars after given fretting cycles were observed and fretting damage mechanisms were analyzed.

2. Experimental Details

Figure 1 shows schematics and photos for an actual fretting wear test apparatus which was used in this work. A typical ACSR 630/45 based on the request of GB/T 1179-2008 [36] was used in this work as it has been widely employed in a high-voltage transmission line and composed of 45 aluminum wires (with 4.22 mm in diameter each). Twenty-one wires were in the outer layer and, among them, 15 wires were in the intermediate layer and the others were in the inner layer. The core of the conductor were constructed by seven steel wires with 2.81 mm in diameter. According to standard GB/T 17048-2009 [37], hard-drawn aluminum wire should have good surface quality without any inappropriate defects. This apparatus was employed based on a servo-controlled fatigue testing machine (MTS 370.10, MTS Systems Corporation, Hennepin, MN, USA). Prior to each test, wire specimens were cleaned in ultrasonic cleaners with alcohol. During the tests, two outer wires were fixed in the spiral groove on the holders. The contact load was generated by the given weight. According to previous study on atmosphere corrosion [38], 0.35 wt % (weight percentage) NaCl solution was used for fretting corrosion test. The solution flowed at a rate of 2.5 mL/min through a rubber pipe, which was adjusted by a clamp prior to fretting tests, and dropped into the contact zone.

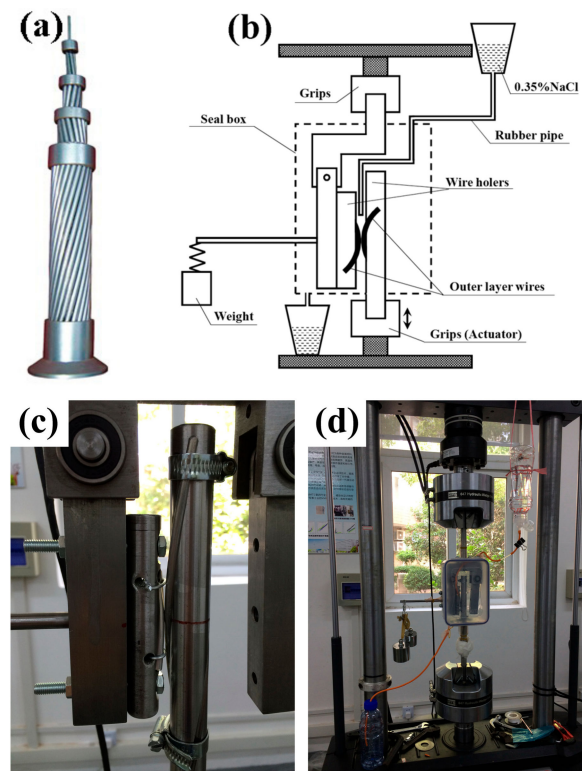


Figure 1. The test apparatus based on MTS 370.10: (a) ACSR 630/45; (b) schematics; (c,d) photos for the actual apparatus.

The following fretting testing parameters were chosen in this work: displacement amplitudes of ± 50 , ± 150 , ± 250 μm ; contact loads (F_n) of 10, 20, 30, and 50 N; frequency of 10 Hz and the number of cycles varying from 1 to 10^5 cycles at room temperature. Deformations on cross-section of specimens under static contact load can be simulated by finite element analysis through ANSYS (ANSYS Inc., Pittsburgh, PA, USA). Figure 2a shows a simplified model used for analysis. The angle between the axes of the two specimens was 21.4° . Young's modulus of 69 GPa and Poisson's ratio of 0.3 were used to calculate. The two rectangular planes were ideally rigid and the rectangular plane of the lower specimen was stable. The loads were applied to the rectangular plane of the upper specimen. Displacement changes of the lower specimen contact surface in load direction with radial distance and axial distance from the contact center were shown in Figure 2b,c. It can be seen that axial distances of contact areas were larger than displacement amplitudes in the fretting tests.

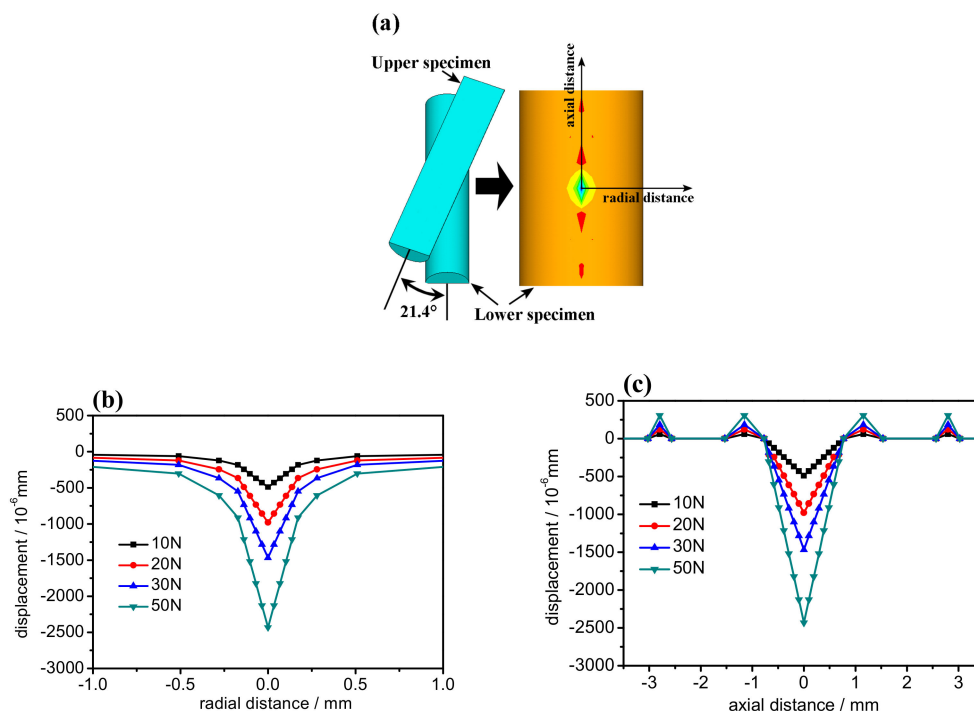


Figure 2. Finite element analysis of contact state: (a) simplify model used, (b) displacement changes in radial direction, and (c) displacement changes in axial direction.

The variety of friction forces (F_t) and displacement amplitude (D) were recorded by a computer, so the fretting running characteristics could be assumed. Morphological observations of the contact marks were carried out using a Hitachi SU-1500 scanning electron microscope (SEM, Hitachi, Tokyo, Japan) after fretting wear tests.

3. Results and Discussion

3.1. Wire Fretting Running Characteristics

Figure 3 shows the fretting running curves of the Al wires under dry friction and in NaCl solution. It can be observed that F_t - D - N curves include three typical fretting regimes—i.e., partial slip regime (straight line), mixed fretting regime (elliptic), and gross slip regime (quasi-rectangular)—which can be found in previous researches about fretting process [9,10]. The variety of fretting regimes according to testing parameters are shown in Table 1. In the dry friction environment, when contact load $F_n = 10$ N (Figure 3a), displacement amplitude $D = \pm 150$ μm . All F_t - D curves are irregular parallelograms, indicating the relative slip occurs between two Al wires. Slip ratio, which is the

ratio of actual sliding distance (AD, Figure 3a) to total displacement, is large and the fretting process is in gross slip regime. In contrast, for $F_n = 20$ N (Figure 3b), the F_t - D curves are changed to an elliptical shape with increasing fretting cycles (about 10^3 to 10^4 cycles), suggesting that the fretting interface has experienced plastic deformation and the fretting process is in mixed regime. The shape of curves is finally stabilized as an irregular parallelogram (about 10^5 cycles). When the contact load exceeds 30 N (Figure 3c) and 50 N (Figure 3d), the F_t - D curves become parallelograms in early period (with fretting cycle about 10 to 10^2 cycles), which are characterized as complete slipping of the contacting wires. With increasing fretting cycle, the F_t - D curve changes to an elliptical shape, which is evidence of the fretting process in a mixed regime. With increasing contact load, the plastic deformation of contact interface occurs much earlier because of higher loads, so that the fretting process changes from a gross slip regime to a mixed one more quickly (10^2 cycles for 30 N, 10 cycles for 50 N). The curve shape is finally stabilized as elliptical loops when $F_n = 50$ N and as irregular parallelogram when $F_n = 30$ N.

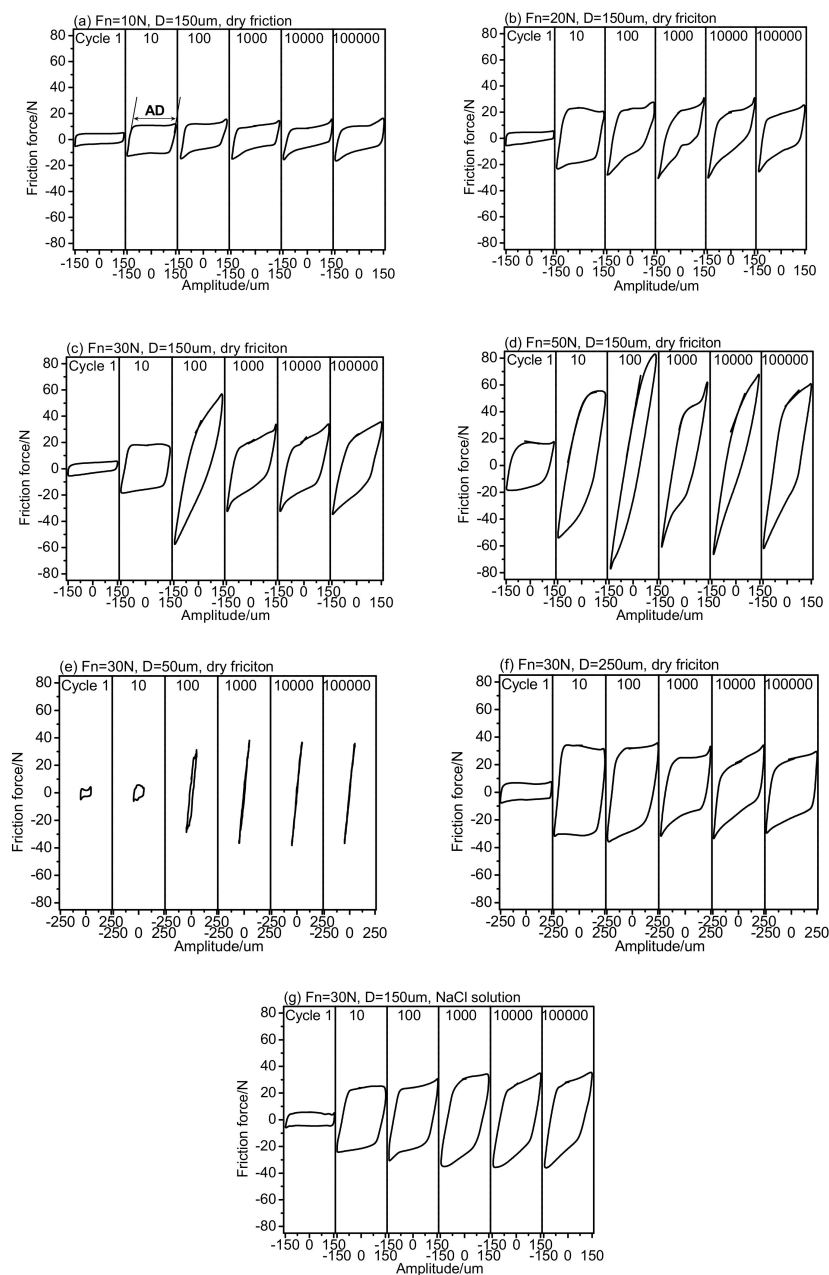


Figure 3. (a–g) Fretting running curve of the Al wires.

Table 1. Distribution of fretting regimes of Al wires. F_n : contact loads; D : displacement amplitude

Condition	10^0	10^1	10^2	10^3	10^4	10^5
$F_n = 10\text{ N}$, $D = 150\ \mu\text{m}$, dry friction	S	S	S	S	S	S
$F_n = 20\text{ N}$, $D = 150\ \mu\text{m}$, dry friction	S	S	S	M	M	S
$F_n = 30\text{ N}$, $D = 150\ \mu\text{m}$, dry friction	S	S	M	S	S	S
$F_n = 50\text{ N}$, $D = 150\ \mu\text{m}$, dry friction	S	M	M	M	M	M
$F_n = 30\text{ N}$, $D = 50\ \mu\text{m}$, dry friction	S	S	P	P	P	P
$F_n = 30\text{ N}$, $D = 250\ \mu\text{m}$, dry friction	S	S	S	S	S	S
$F_n = 30\text{ N}$, $D = 150\ \mu\text{m}$, NaCl solution	S	S	S	S	S	S

Note: P is partial slip regime; M is mixed fretting regime; S is gross slip regime.

When $F_n = 30\text{ N}$, $D = \pm 50\ \mu\text{m}$ (Figure 3e), the F_t - D curves are irregular parallelograms during the early period (about 10 cycles), which illustrate that the relative slip between the wires and fretting process is in gross slip regime. After 100 cycles, all F_t - D curves are in a straight line. Under this condition, the relative motion proceeds by means of surface elastic-plastic deformation. Therefore, the fretting process is in partial slip regime with adhesive wear. As the amplitude D exceeds $\pm 250\ \mu\text{m}$, the friction pairs are in gross slip regime during all test period of time (Figure 3f). However, in the 0.35 wt % NaCl solution (Figure 3g), the F_t - D curves are parallelograms for the entire testing process. This kind of curve shape shows that NaCl solution plays partial role as lubricant in contact surface, which makes fretting process in a full gross slip regime. The distribution of fretting regimes of Al wires under different conditions are summarized in Table 1.

Figure 4 shows the relationship between maximum friction force and fretting cycles under different displacement amplitude (± 50 , ± 150 , $\pm 250\ \mu\text{m}$) and contact loads (10, 20, 30, 50 N). Under dry friction conditions, the maximum friction force is low at the beginning of fretting process (several cycles). Afterwards, the maximum friction force increases sharply and peaks. Subsequently, the maximum friction force drops and stabilizes in the last period.

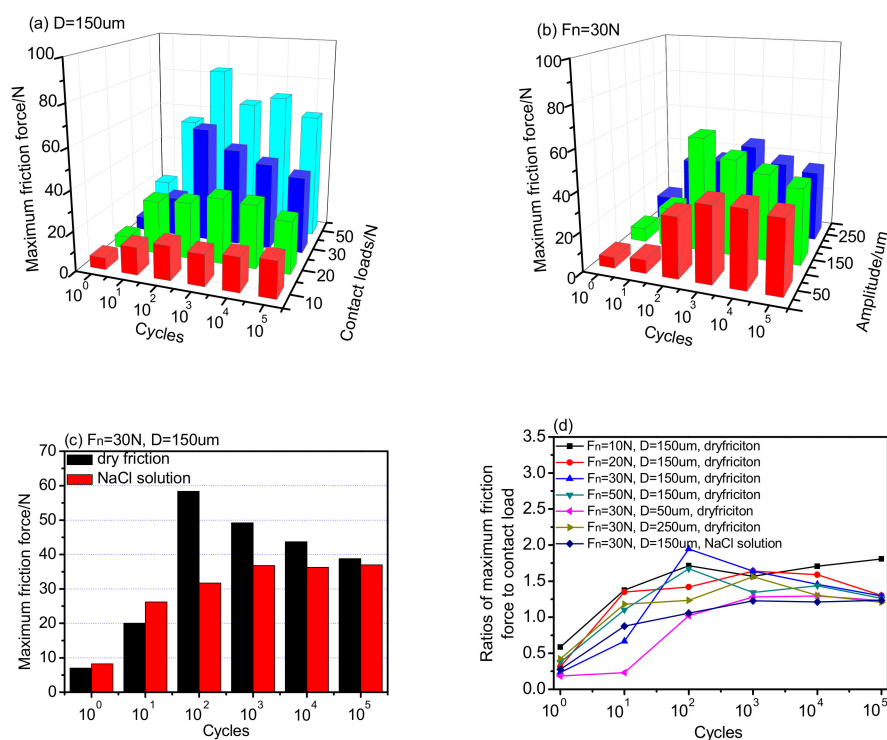


Figure 4. (a–c) The maximum friction force and (d) its ratio to normal force as a function of fretting cycles.

In general, an enhancing contact load induces increasing surface shear stress which shortens maximum friction force stage (Figure 4a). Under low loads (10 N and 20 N), surfaces of the Al wires are subject to elastic deformation, and the contact pressure is relatively small. Under high loads (30 N and 50 N), surfaces of the Al wires experience elastoplastic deformation. When $D = \pm 50 \mu\text{m}$ (Figure 4b), the initial gross slip regime lasts for the first 100 cycles, after which the maximum friction force increases and reach a stable state. For $D = \pm 150 \mu\text{m}$, maximum friction force increases rapidly after running-in stage then decreases slowly. Maximum friction force increases more rapidly when $D = \pm 250 \mu\text{m}$, then stabilized.

It is known that the corrosive medium has a certain influence on the fretting regime. The maximum friction force is relatively smaller in the corrosive medium than in dry friction environment. Under 30 N loads (Figure 4c), maximum friction force in the NaCl solution decreases from 58.4 N (10^2 cycles) to 31.7 N. Figure 4d shows the ratios of the maximum friction force to contact load. With increasing fretting cycle, the ratios increase and reach a stable state after 10 to 10^2 cycles. The ratio under NaCl solution is lower in stable state. After 10^5 cycles, the most ratios reach 1.2 to 1.3, but the ratio is still high when the contact load is 10 N.

3.2. Wear Damage

Figure 5 illustrates the traces of fretting wear scars at different contact loads and displacement amplitudes which were estimated from SEM at low magnification. The scar morphology is typically elliptic. The length and width of the wire contact scar were measured using SEM (Figure 5a) and their values are presented in Figure 6. As seen in Figure 6, the length and width of contact marks increase with increasing contact loads and displacement amplitudes under dry friction environment. Under low loads, fretting interface of Al wires produces elastic deformation only. With increasing contact loads, plastic deformation occurs a certain level on the fretting interface, and the surfaces of Al wires are seriously scratched along with enhancing wear damage (Figure 5a–d).

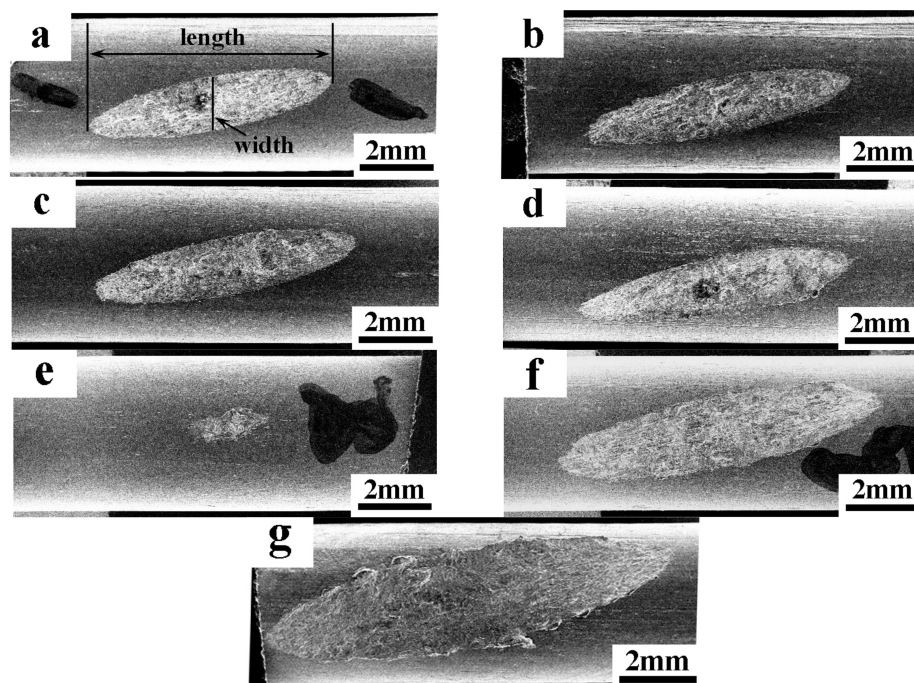


Figure 5. SEM overview of the contact scar on the Al wires: (a) $F_n = 10 \text{ N}$, $D = \pm 150 \mu\text{m}$, dry friction; (b) $F_n = 20 \text{ N}$, $D = \pm 150 \mu\text{m}$, dry friction; (c) $F_n = 30 \text{ N}$, $D = \pm 150 \mu\text{m}$, dry friction; (d) $F_n = 50 \text{ N}$, $D = \pm 150 \mu\text{m}$, dry friction; (e) $F_n = 30 \text{ N}$, $D = \pm 50 \mu\text{m}$, dry friction; (f) $F_n = 30 \text{ N}$, $D = \pm 250 \mu\text{m}$, dry friction; (g) $F_n = 30 \text{ N}$, $D = \pm 150 \mu\text{m}$, NaCl solution.

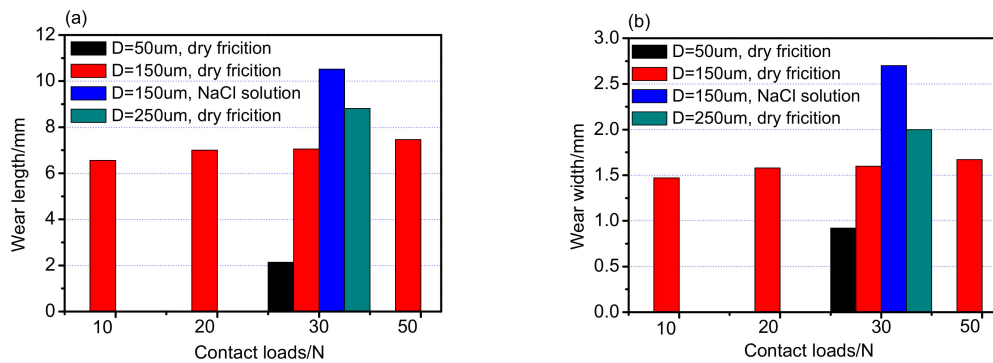


Figure 6. (a) The length and (b) width of contact scar of the fretted wires.

With decreases in displacement amplitudes ($D = \pm 50 \mu\text{m}$), as seen in Figure 5e, the contact mark presents an irregularity morphology of ellipse, where sticking occurs at the fretting interface in the partial slip regime as the above discussion (Figure 3e). With increases in displacement amplitudes ($D = \pm 250 \mu\text{m}$, Figure 5f), the fretting moves up into the gross slip regimes (Figure 3f). The length and width of contact scars increase markedly due to the severe detachment of particles (Figure 6).

In NaCl solution, the length and width of contact scar are larger and more pronounced in the corresponding region (Figure 5g). From the above discussions, NaCl solution plays dual roles as both the lubricant and corrodent. Fretting process of Al wires can be in the gross slip regimes more easily with NaCl “lubricant”. After corrosion, the wear debris is washed by NaCl solution and pitting corrosion occurs on the fretting surface with NaCl “corrodent”.

3.3. Fretting Wear Mechanism

Figure 7 exhibits the SEM morphologies of fretting wear scars under 20 N and 50 N contact load and the displacement amplitude of $\pm 150 \mu\text{m}$. It is noted that the plastic deformation increases evidently with increasing contact load at the edge of fretting wear scar. It is observed that the contact surfaces present plowing along the sliding direction. Some spilled pits can be found on the surface. The results indicate that adhesive wear and abrasive wear are main fretting mechanisms in the conditions mentioned above.

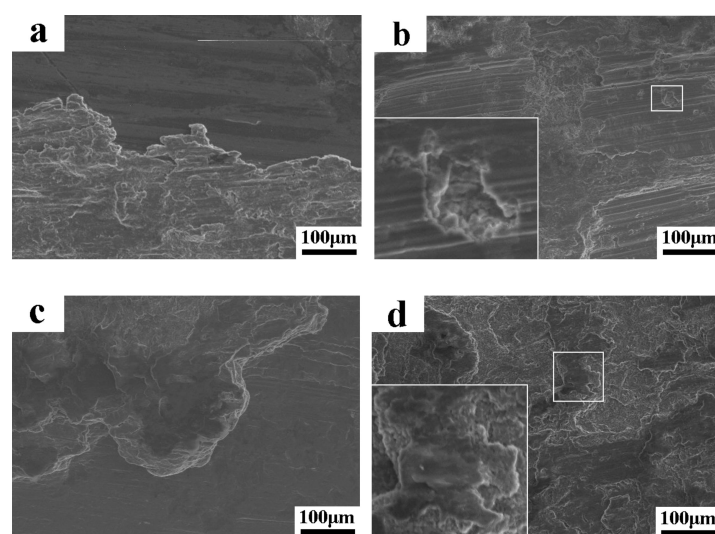


Figure 7. SEM morphologies of fretting wear scars in dry friction environment: (a) $F_n = 20 \text{ N}$, $D = \pm 150 \mu\text{m}$, 10^4 cycles, dry friction; (b) $F_n = 20 \text{ N}$, $D = \pm 150 \mu\text{m}$, 10^5 cycles, dry friction; (c) $F_n = 50 \text{ N}$, $D = \pm 150 \mu\text{m}$, 10^5 cycles, dry friction; (d) $F_n = 50 \text{ N}$, $D = \pm 150 \mu\text{m}$, 10^5 cycles, dry friction.

Figure 8a exhibits severe plastic deformations on fretting contact surfaces, which reveals a typical adhesive characteristic. As the displacement amplitude increases from $\pm 50 \mu\text{m}$ to $\pm 250 \mu\text{m}$, severe plastic deformation, more delaminating and some plowing can be found (Figure 8b,c). As such, the fretting wear mechanisms include adhesive wear and abrasive wear.

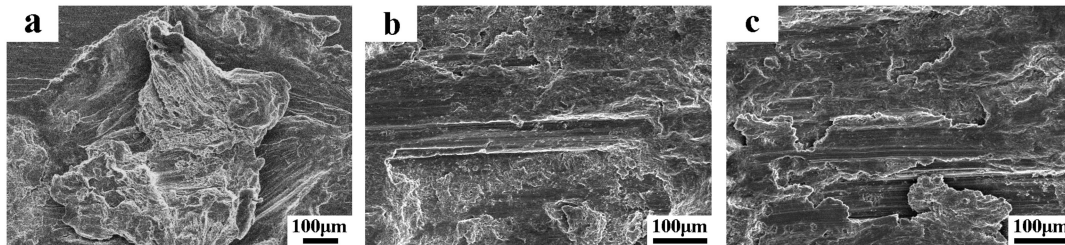


Figure 8. SEM morphologies of fretting wear scars in dry friction environment: (a) $F_n = 30 \text{ N}$, $D = \pm 50 \mu\text{m}$, dry friction; (b) $F_n = 30 \text{ N}$, $D = \pm 250 \mu\text{m}$ dry friction; (c) $F_n = 30 \text{ N}$, $D = \pm 250 \mu\text{m}$ dry friction.

In the NaCl solution, there is no adhesive characteristic on the fretting wear surface. The fretting wear surface is smooth, and some small debris remains on that (Figure 9a). It can be seen from Figure 9b that a small micro-crack is present on surface. This small crack is caused by fatigue as a result of alternating stress during the fretting process. Therefore, fretting wear mechanisms include abrasive wear and fatigue damage.

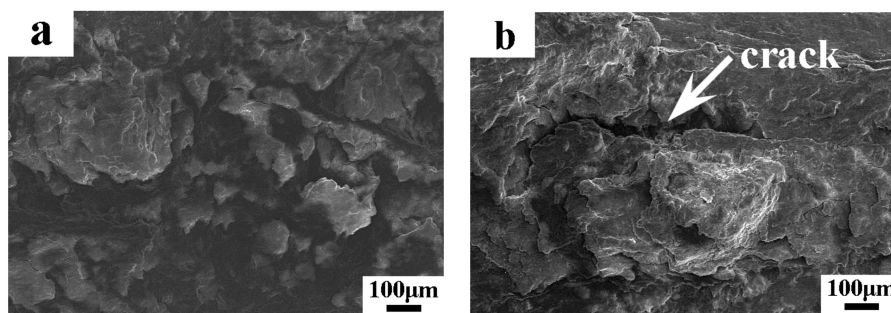


Figure 9. (a,b) SEM morphologies of wear scars in NaCl solution at $F_n = 30 \text{ N}$ and $D = \pm 150 \mu\text{m}$.

4. Conclusions

Based on the laboratory tests, the findings in this work could result in the following conclusions:

- (1) With increasing contact load, the running regime of Al wires changes from a gross slip regime to a mixed regime more quickly. With increasing amplitudes, gross slip regimes are more dominant under 30 N contact loads.
- (2) The corrosive medium has a certain influence on the fretting transition phase. The maximum friction force is relatively smaller in the NaCl solution than in the dry friction environment. At a contact load of 30 N, maximum friction force in the NaCl solution decreases from 58.4 N (10^2 cycles) to 31.7 N, but the wear damage is more serious.
- (3) Abrasive wear and adhesive wear are the main fretting wear mechanisms in the dry friction environments whereas abrasive wear and fatigue damage can be found in the NaCl solution.

Acknowledgments: This work was supported by the National Natural Science Foundation of China (Grant no. 51501108).

Author Contributions: Xingchi Ma conceived and designed the experiments; Xingchi Ma and Lei Gao performed the experiments; Xingchi Ma, Lai-Chang Zhang, and Junxi Zhang. Zhang analyzed the data; Xingchi Ma and Lai-Chang Zhang wrote the paper.

Conflicts of Interest: The authors declare no conflict of interest.

References

1. Kalombo, R.B.; Pestana, M.S.; Ferreira, J.L.A.; da Silva, C.R.M.; Araújo, J.A. Influence of the catenary parameter (H/w) on the fatigue life of overhead conductors. *Tribol. Int.* **2017**, *108*, 141–149. [[CrossRef](#)]
2. Kalombo, R.B.; Araújo, J.A.; Ferreira, J.L.A.; da Silva, C.R.M.; Alencar, R.; Capra, A.R. Assessment of the fatigue failure of an All Aluminium Alloy Cable (AAAC) for a 230 kV transmission line in the Center-West of Brazil. *Eng. Fail. Anal.* **2016**, *61*, 77–87. [[CrossRef](#)]
3. Fadel, A.A.; Rosa, D.; Murça, L.B.; Araújo, J.A. Effect of high mean tensile stress on the fretting fatigue life of an Ibis steel reinforced aluminium conductor. *Int. J. Fatigue* **2012**, *42*, 24–34. [[CrossRef](#)]
4. Azevedo, C.R.F.; Henriques, A.M.D.; Pulino Filho, A.R.; Ferreira, J.L.A.; Araújo, J.A. Fretting fatigue in overhead conductors: Rig design and failure analysis of a Grosbeak aluminium cable steel reinforced conductor. *Eng. Fail. Anal.* **2009**, *16*, 136–151. [[CrossRef](#)]
5. Azevedo, C.R.F.; Cescon, T. Failure analysis of aluminum cable steel reinforced (ACSR) conductor of the transmission line crossing the Paraná River. *Eng. Fail. Anal.* **2002**, *9*, 645–664. [[CrossRef](#)]
6. Aggarwal, R.K.; Johns, A.T.; Jayasinghe, J.A.S.B.; Su, W. An overview of the condition monitoring of overhead lines. *Electr. Power Syst. Res.* **2000**, *53*, 15–22. [[CrossRef](#)]
7. Hur, J.; Kim, K. Investigation on friction and wear of cold rolled high strength steel against an AISI52100 counterpart. *Metals* **2017**, *7*, 90. [[CrossRef](#)]
8. Noraphaiphipaksa, N.; Manonukul, A.; Kanchanomai, C. Fretting fatigue with cylindrical-on-flat contact: Crack nucleation, crack path and fatigue life. *Materials* **2017**, *10*, 155. [[CrossRef](#)] [[PubMed](#)]
9. Zhou, Z.R.; Goudreau, S.; Fiset, M.; Cardou, A. Single wire fretting fatigue tests for electrical conductor bending fatigue evaluation. *Wear* **1995**, *181*, 537–543. [[CrossRef](#)]
10. Zhou, Z.R.; Fiset, M.; Cardou, A.; Cloutier, L.; Goudreau, S. Effect of lubricant in electrical conductor fretting fatigue. *Wear* **1995**, *189*, 51–57. [[CrossRef](#)]
11. Chen, G.H.; Wang, X.; Wang, J.Q.; Liu, J.J.; Zhang, T.; Tang, W.M. Damage investigation of the aged aluminium cable steel reinforced (ACSR) conductors in a high-voltage transmission line. *Eng. Fail. Anal.* **2012**, *19*, 13–21. [[CrossRef](#)]
12. Zhang, D.K.; Feng, C.A.; Chen, K.; Wang, D.G.; Ni, X. Effect of broken wire on bending fatigue characteristics of wire ropes. *Int. J. Fatigue* **2017**, *103*, 456–465. [[CrossRef](#)]
13. Zhang, D.K.; Chen, K.; Zhang, X. Comparison of the thermophysical properties, microstructures, and frictional behavior of lining materials used in mine hoists. *Wear* **2016**, *354*, 1–9. [[CrossRef](#)]
14. Zhang, D.K.; Geng, H.; Zhang, Z.F.; Wang, D.G.; Wang, S.Q.; Ge, S.R. Investigation on the fretting fatigue behaviors of steel wires under different strain ratios. *Wear* **2013**, *303*, 334–342. [[CrossRef](#)]
15. Zhang, D.K.; Chen, K.; Jia, X.F.; Wang, D.G.; Wang, S.Q.; Luo, Y.; Ge, S.R. Bending fatigue behaviour of bearing ropes working around pulleys of different materials. *Eng. Fail. Anal.* **2013**, *33*, 37–47. [[CrossRef](#)]
16. Zhang, D.K.; Shen, Y.; Xu, L.M.; Ge, S.R. Fretting wear behaviors of steel wires in coal mine under different corrosive mediums. *Wear* **2011**, *271*, 866–874. [[CrossRef](#)]
17. Chen, Y.; Zhang, J.X.; Dai, N.W.; Qin, P.; Attar, H.; Zhang, L.-C. Corrosion Behaviour of Selective Laser Melted Ti-TiB Biocomposite in Simulated Body Fluid. *Electrochim. Acta* **2017**, *232*, 89–97. [[CrossRef](#)]
18. Dai, N.W.; Chen, Q.M.; Zhang, J.X.; Zhang, X.; Ni, Q.Z.; Jiang, Y.M.; Li, J. The corrosion behavior of steel exposed to a DC electric field in the simulated wet-dry cyclic environment. *Mater. Chem. Phys.* **2017**, *192*, 190–197. [[CrossRef](#)]
19. Hoseinie, S.M.; Homborg, A.M.; Shahrabi, T.; Mol, J.M.C.; Ramezanzadeh, B. A Novel Approach for the Evaluation of Under Deposit Corrosion in Marine Environments Using Combined Analysis by Electrochemical Impedance Spectroscopy and Electrochemical Noise. *Electrochim. Acta* **2016**, *217*, 226–241. [[CrossRef](#)]
20. Otieno, M.; Beushausen, H.; Alexander, M. Chloride-induced corrosion of steel in cracked concrete—Part I: Experimental studies under accelerated and natural marine environments. *Cem. Concr. Res.* **2016**, *79*, 373–385. [[CrossRef](#)]
21. Dai, N.W.; Zhang, L.-C.; Zhang, J.X.; Chen, Q.M.; Wu, M.L. Corrosion behavior of selective laser melted Ti-6Al-4V alloy in NaCl solution. *Corros. Sci.* **2016**, *102*, 484–489. [[CrossRef](#)]

22. Sambyal, P.; Ruhi, G.; Dhawan, R.; Dhawan, S.K. Designing of smart coatings of conducting polymer poly (aniline-co-phenetidine)/SiO₂ composites for corrosion protection in marine environment. *Surf. Coat. Technol.* **2016**, *303*, 362–371. [[CrossRef](#)]
23. Dai, N.W.; Zhang, L.-C.; Zhang, J.X.; Zhang, X.; Ni, Q.Z.; Chen, Y.; Wu, M.L.; Yang, C. Distinction in corrosion resistance of selective laser melted Ti-6Al-4V alloy on different planes. *Corros. Sci.* **2016**, *111*, 703–710. [[CrossRef](#)]
24. Caines, S.; Khan, F.; Shirokoff, J.; Qiu, W. Experimental design to study corrosion under insulation in harsh marine environments. *J. Loss Prev. Process Ind.* **2015**, *33*, 39–51. [[CrossRef](#)]
25. Guo, A.X.; Li, H.T.; Ba, X.; Guan, X.C.; Li, H. Experimental investigation on the cyclic performance of reinforced concrete piers with chloride-induced corrosion in marine environment. *Eng. Struct.* **2015**, *105*, 1–11. [[CrossRef](#)]
26. Wasim, M.; Hussain, R.R. Passive film formation and corrosion initiation in lightweight concrete structures as compared to self compacting and ordinary concrete structures at elevated temperature in chloride rich marine environment. *Constr. Build. Mater.* **2015**, *78*, 144–152. [[CrossRef](#)]
27. Lu, Z.; Wang, P.; Zhang, D. Super-hydrophobic film fabricated on aluminium surface as a barrier to atmospheric corrosion in a marine environment. *Corros. Sci.* **2015**, *91*, 287–296. [[CrossRef](#)]
28. Dai, N.W.; Zhang, J.; Chen, Y.; Zhang, L.C. Heat treatment degrading the corrosion resistance of selective laser melted Ti-6Al-4V alloy. *J. Electrochem. Soc.* **2017**, *164*, C428–C434. [[CrossRef](#)]
29. Ilo, K.C.; Derby, E.J.; Whittaker, R.K.; Blunn, G.W.; Skinner, J.A.; Hart, A.J. Fretting and Corrosion Between a Metal Shell and Metal Liner May Explain the High Rate of Failure of R3 Modular Metal-on-Metal Hips. *J. Arthroplast.* **2017**, *32*, 1679–1683. [[CrossRef](#)] [[PubMed](#)]
30. Li, J.; Yang, B.B.; Lu, Y.H.; Xin, L.; Wang, Z.H.; Shoji, T. The effect of normal force on fretting corrosion behavior of Inconel 690 in 3.5% sodium chloride. *Mater. Charact.* **2017**, *131*, 224–233. [[CrossRef](#)]
31. Sawada, T.; Schille, C.; Almadani, A.; Geis-Gerstorf, J. Fretting Corrosion Behavior of Experimental Ti-20Cr Compared to Titanium. *Materials* **2017**, *10*, 194. [[CrossRef](#)] [[PubMed](#)]
32. Sato, Y.; Iwabuchi, A.; Uchidate, M.; Yashiro, H. Dynamic corrosion properties of impact–fretting wear in high-temperature pure water. *Wear* **2015**, *330–331*, 182–192. [[CrossRef](#)]
33. Bryant, M.; Farrar, R.; Freeman, R.; Brummitt, K.; Newille, A. Fretting corrosion characteristics of polished collarless tapered stems in a simulated biological environment. *Tribol. Int.* **2013**, *65*, 105–112. [[CrossRef](#)]
34. Swaminathan, V.; Gilbert, J.L. Fretting corrosion of CoCrMo and Ti6Al4V interfaces. *Biomaterials* **2012**, *33*, 5487–5503. [[CrossRef](#)] [[PubMed](#)]
35. Vera, R.; Delgado, D.; Rosales, B.M. Effect of atmospheric pollutants on the corrosion of high power electrical conductors: Part 1. Aluminium and AA6201 alloy. *Corros. Sci.* **2006**, *48*, 2882–2900. [[CrossRef](#)]
36. GB/T 1179-2008. *Round Wire Concentric Lay Overhead Electrical Wired Conductors (IEC 61089: 1991, MOD)*; Standardization Administration of the People’s Republic of China: Beijing, China, 2008; pp. 1–36.
37. GB/T 17048-2009. *Hard-Drawn Aluminium Wire for Overhead Line Conductors (IEC 60889: 1987)*; Standardization Administration of the People’s Republic of China: Beijing, China, 2009; pp. 1–5.
38. Yuan, X.J.; Zhang, J.X.; Chen, Q.M.; Tan, T.; Ma, X.C. Electrochemical process of Zn electrode covered with thin electrolyte layer under external electric field. *Corros. Sci. Protect. Technol. China* **2014**, *26*, 197–204. [[CrossRef](#)]

